Materials Advances

ROYAL SOCIETY OF CHEMISTRY

PAPER

View Article Online
View Journal

Cite this: DOI: 10.1039/d6ma00220j

In silico design to explore the effect of the metalloporphyrin and C_{60} cage on non-linear optical (NLO) properties

Shama Rafiq,[a] Nimra Sultan [a] and Muhammad Ramzan Saeed Ashraf Janjua *[ab]

Received 16th February 2026,
Accepted 31st March 2026

DOI: 10.1039/d6ma00220j

rsc.li/materials-advances

The uses of nonlinear optical (NLO) materials in photonics, optoelectronics, optical switching, and data storage have drawn a lot of interest. This work provides a theoretical analysis of how the Zn-porphyrin and fullerene (C_{60}) cage affect the NLO characteristics of four designed systems: **MP1**, **MP2**, **MP1C60**, and **MP2C60**. To optimize molecular geometries and assess important parameters like HOMO–LUMO energy gaps, dipole polarizability, and first-order hyperpolarizability, density functional theory (DFT) calculations using the B3LYP functional were utilized. **MP2** showed improved charge delocalization with the smallest energy gap (0.376 eV). Fullerene's function as an efficient electron acceptor was confirmed by functionalization with C_{60}, which changed the electronic distributions in **MP1C60** and **MP2C60**. Structural stability was demonstrated by the Zn–N bond lengths remaining constant at 2.07 nm. Significant improvements were seen in polarizability and hyperpolarizability, especially for **MP2C60** (β_{total} = 78 128.92 × 10^{-30} esu). According to these results, the metalloporphyrin and C_{60} work in concert to significantly enhance NLO performance, making these hybrids attractive options for cutting-edge photonic and optoelectronic applications.

1. Introduction

In recent decades, the scientific discipline of non-linear optics has experienced remarkable growth. It is predicated on the phenomenon of powerful coherent light radiation interacting with matter. The study of how light interacts with matter in situations where the atoms' non-linear response is significant is known as non-linear optics.[1] Organic compounds with NLO properties became unmatched in popularity and dominance in a variety of fields, including medicine, materials science, atomic, molecular, and solid-state physics, surface interface sciences, and chemical dynamics, as a result of the quick development of high-tech electronic, optical, and storage devices.[2,3] Many materials, including graphene,[4,5] fullerene,[6] and quantum dots,[7,8] have garnered scientific interest in recent decades due to their noteworthy nonlinear optical (NLO) characteristics. The study of organic and organometallic chromophores has also received a great deal of attention. In these cases, nonlinearity is primarily caused by the so-called push–pull architecture, which consists of a donor and an acceptor moiety connected by a π-delocalized spacer.[9] The NLO characteristics of the fundamental molecules dictate the NLO characteristics of the materials. Modeling organic molecules with high NLO characteristics is beneficial when using this criterion.[10,11] Appropriate donor–π-spacer–acceptor (D–π–A) systems with structurally modifiable features are required to model and build high-response NLO materials. In this way, substitution is a key component in the conjugation modification and, consequently, the NLO activity.[12,13] A lot of work has gone into developing very effective NLO materials. It is commonly recognized that altering the donor and acceptor capacities and prolonging the π-conjugated bridge can control the molecular second-order NLO characteristics. The electronic intramolecular charge transfer (ICT) of the molecule is linked to the initial hyperpolarizability and, consequently, the second-order NLO response.[14,15]

Because of their structural diversity and ease of chemical alteration, porphyrins and metalloporphyrins are frequently employed as field-responsive materials in optoelectronics. Their ligands are useful for nonlinear optical applications because they offer significant dipole moments, polarizability, and hyperpolarizability. The potential of polymeric porphyrins in innovative materials applications is increased by their remarkable low-dimensional conductivity.[16] Porphyrins have garnered a lot of interest as an organic material with elevated nonlinear optical susceptibility in the hunt for better third-order nonlinearity materials because of their large p-electron

[a] Department of Chemistry, Government College University Faisalabad, Faisalabad, 38000, Pakistan. E-mail: Janjua@gcuf.edu.pk, Dr_Janjua2010@yahoo.com; Tel: +92 300 660 49 48
[b] Research Center for Crystal Materials, CAS Key Laboratory of Functional Materials and Devices for Special Environments, Xinjiang Technical Institute of Physics and Chemistry, CAS, 40-1 South Beijing Road, Urumqi, 830011, P.R. China

systems with 2D conjugated molecular arrangements as well as the presence of 1D delocalized electrons.[17] Because of their high solubility, probable processability as layers, and thermal and chemical durability, 2D structures based on delocalized macrocycles, including porphyrins and metal porphyrins, have garnered a lot of interest.[18] Furthermore, they can easily create an electronic exchange in a push–pull system by using their polarizable conjugated ring as a linker, which is necessary for a significant second-order NLO response.[19] To create different donor–(π-conjugated bridge)–acceptor (D–π–A) and D–π–D systems, porphyrins and metalloporphyrins can be utilized as π-conjugated bridges.[20,21] Previous research showed that metal complexation and the type of suitable donor–acceptor substituents can readily adjust the NLO characteristics of porphyrins.[22–24]

A network of fused carbon atoms forms a spherical carbon cage known as a fullerene. Specifically, C_{60} fullerene is made up of 60 carbon atoms organized in a highly symmetrical configuration.[25] Since buckminsterfullerene (C_{60}) characterization, fullerene and its derivatives have garnered a lot of attention due to their special physicochemical characteristics, which are helpful in a variety of materials science applications.[26–28] The polyhedral counterparts of two-dimensional graphene sheets are called fullerenes. Though in trace proportions, they have been found in interplanetary space and are found in nature.[29–31] Because of its distinct physical and molecular characteristics, C_{60} has garnered a lot of scientific attention.[32] The most significant features of C_{60} are by far its extremely symmetric structure, its capacity for multiple addition processes, and its remarkable electron-accepting capabilities (*e.g.*, it can take on up to six electrons).[33] A number of applications are still in their infancy, and fullerenes have only lately been employed in innovative optical applications, cancer therapy, and noninvasive cancer imaging. Future studies will examine the use of fullerene C_{60} in catalysis, water purification, biohazard prevention, portable electricity, automobiles, and medicine.[34]

Nanostructured thin films with tunable sizes enable charge carrier confinement, making them essential for optoelectronic applications.[35] Various advanced materials, including rare-earth-doped upconversion systems, polyoxometalates, metal nanoclusters, and cage-cluster frameworks, have been explored for nonlinear optical (NLO) applications due to their unique optical and electronic properties; however, some are limited by low efficiency or slow development.[36–39] In particular, Ag/Au nanoclusters and silver alkynyl systems exhibit strong quantum confinement and ultrafast response, making them promising for optoelectronic and all-optical switching applications.[38,40] Additionally, switchable NLO materials based on redox and photoresponsive mechanisms have gained attention for electro-optic applications.[41] Experimental studies, such as femtosecond Z-scan on TiO_2 nanoparticles, further confirm strong NLO responses, highlighting the broad potential of these materials in advanced photonic technologies.[42]

We are now working to ascertain the hybrid composites' NLO responses to metalloporphyrin–C_{60} cages. To put it briefly, we have theoretically created four hybrid composites using Zn-porphyrins and C_{60} fullerenes in our research. We employed DFT calculations to forecast these composites' NLO response. In order to investigate the suggested molecules' NLO response, a number of metrics have been calculated, including linear polarizability, second-order nonlinearity, HOMO–LUMO gap, and charge transfer mechanism. For upcoming photonic and electronic devices, these hybrid materials might provide strong and adjustable NLO responses. The intelligent development of future optical materials can be guided by this method.

2. Computational insights

Gaussian 09 computational software is used to carry out the density functional theory (DFT) calculations.[43] Of the several DFT techniques that are available, we have chosen the B3LYP method,[44] which combines the Lee, Yang, and Parr correlation functional (LYP) with Becke's three-parameter hybrid exchange functional (B3).[45] In addition, B3LYP is accessible in the majority of quantum chemistry software packages and is quite simple to use.[46] Because of its accuracy in forecasting molecule structures and other properties, B3LYP is used in computational chemistry simulations in conjunction with the 6-311G basis set. Geometry optimization was performed using DFT theory at the B3LYP/6-31G* level.[47]

Finding the smallest point of energy is the aim of geometric optimization calculations since it represents the actual molecular structure and is used to compute bond length, bond angle, and other characteristics. The 6-311*G basis set was found to be appropriate for the H, O, and N atoms,[48] while LANL2DZ (Los Alamos National Laboratory 2-double-z) associated with pseudo-potential was used for zinc (Zn). Selecting an appropriate model and calculation technique is essential for quantum chemical research in order to gather precise data and comprehend the connection between the computed outcomes and physical characteristics. The B3LYP approach is appropriate for fullerene systems since several groups have used it and obtained satisfactory findings, and density functional theory is used extensively in calculations because of its rather acceptable accuracy and affordable cost.[49–51] Additionally, the NLO properties of the optimized molecules were taken into account. Using the same level of the basis set and functional used for optimization, the first hyperpolarizabilities for each chemical system were found to determine the NLO characteristics. To further comprehend the charge transfer process in the investigated push–pull compounds, HOMO–LUMO analysis was also carried out.

First-order polarizability and first-order hyperpolarizability were examined using an additional computational approach. The following formulas are used to determine hyperpolarizability $\langle\beta\rangle$ and polarizability $\langle\alpha\rangle$. First-order polarizability is computed using eqn (1):[52]

$$\langle a\rangle = 1/3(a_{xx} + a_{yy} + a_{zz}), \quad (1)$$

whereas for the calculation of first-order hyperpolarizability, we use eqn (2):[53]

$$\langle\beta\rangle = (\beta_x{}^2 + \beta_y{}^2 + \beta_z{}^2)^{1/2}$$

where $\beta_x = \beta_{xxx} + \beta_{xyy} + \beta_{xzz}$, $\beta_y = \beta_{yyy} + \beta_{xxy} + \beta_{yzz}$, $\beta_z = \beta_{zzz} + \beta_{xxz} + \beta_{yyz}$

$$\beta_{tot} = [(\beta_{xxx} + \beta_{xyy} + \beta_{xzz})^2 + (\beta_{yyy} + \beta_{xxy} + \beta_{yzz})^2 + (\beta_{zzz} + \beta_{xxz} + \beta_{yyz})^2]^{1/2} \quad (2)$$

For a deeper understanding of the process of nonlinear polarization, we first consider first-order polarizability (α), which represents an estimate of the degree of linear polarization under the influence of an electrical field. We have calculated the values of the first-order polarizability (α) components for each compound using eqn (1). The magnitude of first-order hyperpolarizability is calculated using eqn (2).

3. Geometric structure

Based on the Zn-porphyrin (Zn-P) and carbon 60 cage shown in Fig. 1, we have created four push–pull molecules (**MP1**, **MP2**, **MP1C60**, and **MP2C60**) using DFT insights. The optimized bond distances are provided in Table 1. The zinc-porphyrin core that serves as the main light-harvesting donor is the foundation of these four systems. The efficiency of charge transfer from the donor to the fullerene acceptor can be predicted by methodically altering the linkers and peripheral groups.[54]

Table 1 Computed bond lengths in nm for all four designed compounds

Geometrical parameters	MPPP1	MPPP2	MPPP1C_{60}	MPPP2C_{60}
Zn–N	2.07 (2.0)*	2.07	2.07	2.07

We selected zinc (Zn) porphyrin and fullerene (C_{60}) for their efficient donor–bridge–acceptor (D–π–A) system, where a conjugated π-spacer facilitates rapid intramolecular charge transfer (ICT). This architecture promotes extensive electron redistribution under light, yielding high polarizability and enhanced second- and third-order hyperpolarizabilities, making the composite suitable for optical limiting, frequency modulation, and high-speed switching.

In **MP1**, there is a charge shift from Zn-porphyrin to the aromatic rings, indicating that the aromatic rings act as an electron attractor or acceptor and the Zn-porphyrin cage as an electron donor. TTF-based donor substituents that are affixed to the porphyrin framework in **MP2** improve intramolecular charge transfer and electron-donating capacity. The aromatic rings serve as an electron donor for **MP1C60** and **MP2C60**, while the fullerene cage acts as an electron acceptor.

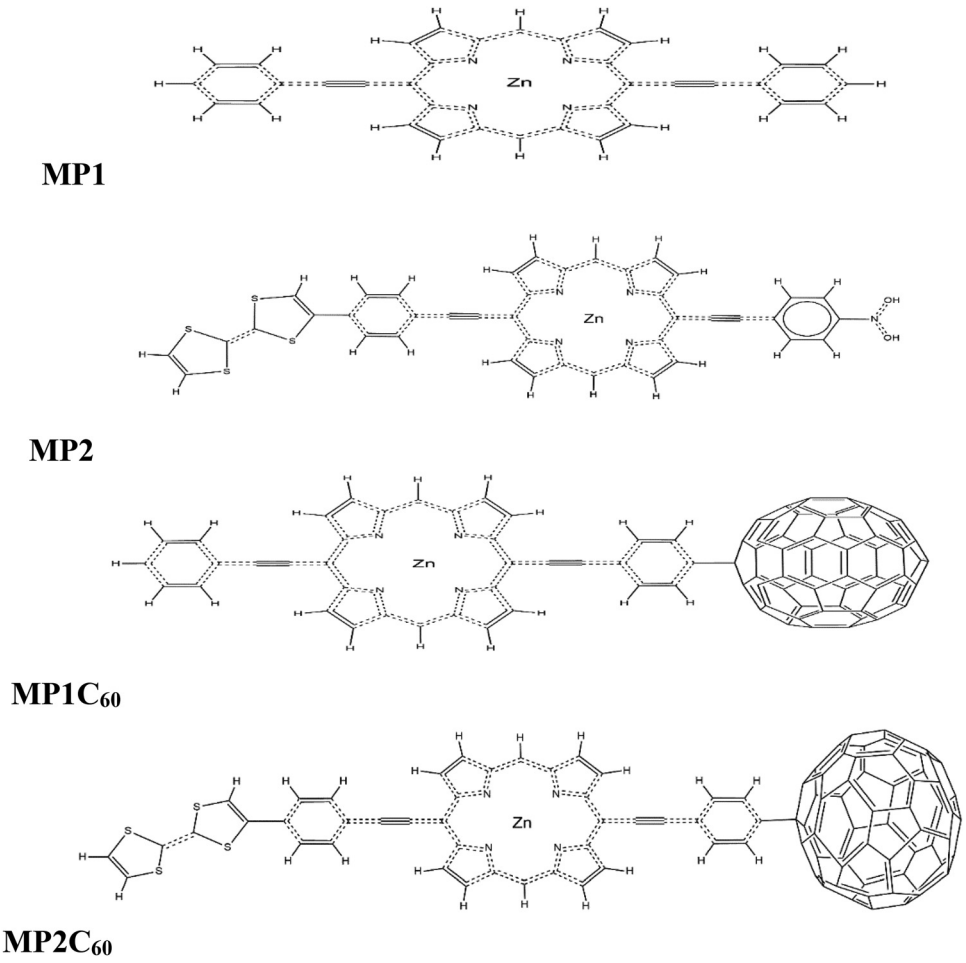

Fig. 1 Chemical structures of the investigated systems: **MP1**, **MP2**, **MP1C60** and **MP2C60**.

Adding another fullerene to the opposite side of **MP2C60** would create a symmetric acceptor system, which could reduce directional intramolecular charge transfer (ICT) and partially lower nonlinear optical (NLO) efficiency. However, depending on conjugation and orbital alignment, it might enhance light absorption or stabilize excited states, so the overall NLO response would depend on molecular symmetry, orbital distribution, and electronic coupling.

When compared to porphyrin alone, the nonlinear optical (NLO) capabilities are greatly enhanced by the presence of fullerene. Although **MP1C60** is a small and effective model for quick electron transport, **MP2C60** functions as a more potent "molecular wire" thanks to its longer bridge. This **MP2C60** is intended to optimize the nonlinear optical response, thereby creating a more potent contender for laser protection and high-performance photonic devices.

4. Results and discussion

To investigate the NLO response of the suggested molecules, a few metrics were calculated, including linear polarizability, second-order nonlinearity, HOMO–LUMO gap, and charge transfer mechanism. To characterize the chemical reactivity of the hybrid compounds, we have first described the HOMO–LUMO energy differential displayed in Fig. 2. All the compounds have smaller energy gaps, which suggests that there is a substantial charge transfer between the molecules. The easier the charge transfer, the smaller the energy gap between the HOMO and LUMO. Table 2 shows the HOMO–LUMO energy difference.

The designed molecules have HOMO energies between −10.877 and −8.220 eV and LUMO values between −9.796 and −7.507 eV. One crucial indicator of intramolecular charge transfer effectiveness and molecular electronic softness is the shrinking HOMO–LUMO energy gap. The magnitude of the electronic transmission between these units determines the bandgap. The non-linear variation in gap values can be caused by various linkers, such as ethynylenephenylene, which can either help or hinder this coupling. **MP1** has the largest energy gap (1.081 eV) of any system under study, which suggests comparatively poorer electronic polarizability and charge transfer capacity. **MP2**, on the other hand, exhibits the lowest bandgap (0.436 eV), indicating better electronic delocalization and increased charge transport inside the molecular structure.

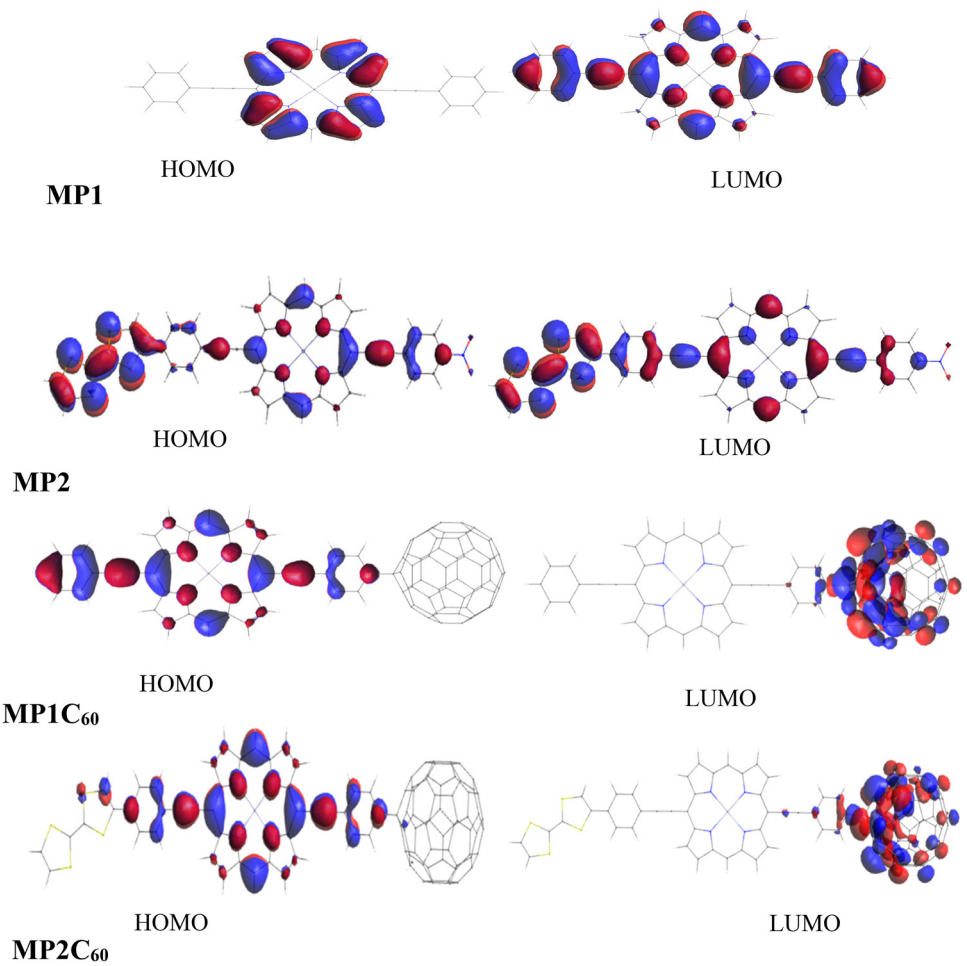

Fig. 2 The frontier molecular orbitals of four designed molecules involved in the dominant electron transitions.

Table 2 Computed HOMO–LUMO energy difference (eV) for the designed molecules

Compound	MP1	MP2	MP1C60	MP2C60
E_{HOMO} (eV)	−10.877	−9.369	−9.162	−8.220
E_{LUMO} (eV)	−9.796	−8.933	−8.244	−7.507
$\Delta E = E_{LUMO} - E_{HOMO}$ (eV)	1.081	0.436	0.918	0.714

MP2 has tetrathiafulvalene (TTF) derivatives (the sulfur-containing rings on the left), which contribute to the lower bandgap. Due to their minimal energy gap and intramolecular charge transfer (ICT), TTF derivatives are incredibly potent electron donors.[55] An extremely delocalized ''electronic highway'' can go throughout the entire molecule, thanks to the structure of **MP2**. The ''ground state'' (HOMO) and ''excited state'' (LUMO) have very little energy difference when electrons are allowed to flow around a flat, conjugated system.

The complexes **MP1C60** and **MP2C60**, which include fullerene, have intermediary bandgap values of 0.918 eV and 0.714 eV, respectively. As demonstrated in porphyrin–fullerene hybrid materials, where the LUMO and HOMO are specifically localized on the acceptor/donor parts of the molecule, the presence of an electron acceptor, such as fullerene, in D–A systems tunes frontier orbital energies and leads to charge transfer properties that affect nonlinear optical response.[33] Because of the steric barrier caused by the bulky fullerene's attachment, these complexes have a greater bandgap than **MP2**. By altering the orbitals' planar alignment and decreasing the effective conjugation, this crowding can distort the molecular structure and increase the HOMO–LUMO gap. Because **MP2C60** retains the TTF-like donor groups from **MP2**, which are far more potent donors than the straightforward phenyl/alkyne groups in **MP1C60**, its bandgap is lower than that of **MP1C60**. Overall, the decreasing bandgap trend follows the order:

$$\textbf{MP1} > \textbf{MP1C60} > \textbf{MP2C60} > \textbf{MP2}.$$

Fig. 2 displays the chemical orbitals involved in these four molecules' main electron transitions.

Examining the physical mechanism pertaining to the determination of the first-order polarizability (a) is equally crucial for the consideration of the first-order hyperpolarizability (β). First-order polarizability is calculated using eqn (1). Table 3 shows the calculated dipole polarizability coefficients of the four compounds.

The first-order polarizability tensors a_{ii} ($i = x, y, z$) for the four chosen molecules are nonzero. According to the polarizability tensor study, **MP2**, **MP1C60**, and **MP2C60** show the highest polarizability along the x-axis, suggesting that the molecular backbone is where the majority of electron delocalization and charge transfer takes place. Conversely, **MP1** exhibits more polarizability along the y-axis, indicating a distinct electron density distribution and much less longitudinal conjugation. Fullerene's attachment improves directional charge transfer along the x-axis because of its strong donor–acceptor interaction and extended π-conjugation.

Table 3 First-order polarizability elements (in 1×10^{-30} esu) for the four designed compounds

Comp.	a_{xxx}	a_{yyy}	a_{zzz}	$\langle a \rangle$
MP1	4.57	20.58	1.08	8.74
MP2	52.12	5.98	1.62	19.91
MP1C60	28.59	8.49	5.07	14.05
MP2C60	136.55	9.83	5.81	50.73

The HOMO–LUMO bandgap and polarizability are typically inversely correlated in molecular systems.[56] Ahsin *et al.* (2024) established that polaron formation in conducting polymers induces a significant reduction in the HOMO–LUMO energy bandgap (ΔE), resulting in a dramatic increase in the first hyperpolarizability (β). This robust inverse relationship, where decreased excitation energy leads to enhanced nonlinear optical (NLO) response, shows β values increasing by up to 246 times in polaronic states.[57] An external electric field can more readily deform electrons with a smaller energy gap because they are less firmly attached to the nuclei. For example, **MP2**'s average polarizability is 19.91 compared to 8.74, a direct result of its substantially shorter bandgap (0.436) than that of **MP1** (1.081). Polarizability increases with molecular size and the degree of π-conjugation according to structural analysis. By adding the big, electron-dense C_{60} fullerene cage to the porphyrin structures, a vast reservoir of non-alignable electrons is created, which increases the first-order polarizability values by ''stretching'' the electron cloud.

Electrons can move along the whole length of the TTF derivative, porphyrin, and fullerene units in long, linear molecules like the **MP2C60** triad. Adding groups like fullerenes can occasionally increase the bandgap by stabilizing the molecule's ground state, but first-order polarizability is higher than that of all other compounds. Historically, the molecules have been divided into two categories: orbital controlled (soft-type) and charge controlled (hard-type). The soft type relies on a molecule's capacity to transfer charge either instantly or permanently, whereas the hard-type relies on the molecule's uneven charge distribution. Due to their increased sensitivity to external perturbations, the border molecular orbitals are particularly implicated in soft-type interactions.[58] Despite having more electrons and being a bigger molecule, **MP1C60**'s bandgap (0.918 eV) is more than double that of **MP2** (0.436 eV). The increased excitation energy needed for **MP1C60** produces a relatively stiff electron cloud that is less sensitive to an external electric field since polarizability and bandgap are negatively correlated. On the other hand, **MP2**'s electron cloud is more flexible and easily polarizable due to its narrower bandgap, which makes electrical excitation simpler. As a result, **MP1C60** has a rather hard molecular nature with little electron cloud deformability, while **MP2** has a softer molecular nature with better intramolecular charge transfer and increased polarizability. The first-order polarizability of the four designed molecules decreases in the following order:

$$\textbf{MP2C60} > \textbf{MP2} > \textbf{MP1C60} > \textbf{MP1}$$

Table 4 shows the total hyperpolarizability (β_{tot}) and the calculated first-order hyperpolarizability tensor components

Table 4 Computed values of first-order hyperpolarizability tensors (1×10^{-30} esu) for all the compounds

Tensors	MP1	MP2	MP1C60	MP2C60
β_{xxx}	0.00003917	−1418.692	−5702.829	78 021.079
β_{xxy}	0.00070914	104.031	−10.591	−2395.119
β_{xyy}	−0.003496	28.205	−8.881	20.642
β_{yyy}	0.003226	2.266	0.538	10.432
β_{xxz}	0	−14.797	107.097	2315.702
β_{yyz}	0	− 0.353	−1.787	−2.881
β_{xzz}	−0.00000339	−0.918	0.10038	16.416
β_{yzz}	0.000000332	0.0257	−0.752	−1.765
β_{zzz}	0	0.013	5.006	2.391
β_{tot}	0.00524	1395.54	5712.68	78 128.92

(β_{xxx}, β_{xxy}, β_{xyy}, *etc.*) for **MP1**, **MP2**, **MP1C60**, and **MP2C60** calculated using eqn (2).

Following the order **MP1** ≪ **MP2** < **MP1C60** ≪ **MP2C60**, the calculated first-order hyperpolarizability (β_{tot}) exhibits a noticeable increase across the systems under study. Because polarizability and first-order hyperpolarizability reflect essentially different ways that molecules react to an electric field, their values do not follow the same upward trend. As molecules become larger from **MP1** to **MP2C60**, polarizability (α), a linear property, increases proportionally with the molecular volume and total amount of electrons.

The first-order hyperpolarizability, on the other hand, is a nonlinear feature that only depends on the extent of intramolecular charge transfer (ICT) and structural asymmetry. First-order hyperpolarizability needs a "push–pull" system in which an electron-donating group is joined to an electron-accepting group by a conjugated bridge, whereas polarizability only needs room for electrons to move. Compared to systems incorporating fullerene, **MP1** and **MP2** exhibit reduced hyperpolarizability due to their stiffer electron clouds, absence of prolonged π-conjugation, and limited intramolecular charge transfer. The enhanced hyperpolarizability (β) of **MP2** relative to **MP1**, prior to fullerene attachment, arises from the presence of a stronger electron-donating TTF derivative, which increases intramolecular charge transfer and extends π-conjugation within the molecular framework. The sulfur-containing rings improve electron delocalization and polarizability due to their higher electron density and polarizable nature, leading to greater charge separation under an applied electric field. In contrast, the phenyl groups in **MP1** exhibit comparatively weaker electron-donating ability and limited conjugation efficiency. As a result, **MP2** demonstrates a more pronounced nonlinear optical response than **MP1** even before the incorporation of fullerene C_{60}, highlighting the intrinsic contribution of its molecular architecture to the observed increase in β.

C_{60} is a common compound used in multicomponent molecular architecture to adjust its optical properties to certain spectral regions of interest because of its high electron-accepting capabilities and exceptionally small reorganization energy (*ca.* 0.23 eV). By employing chemical techniques, the average hyperpolarizabilities in fullerene derivatives are greatly enhanced by the C_{60} moiety, which functions as an electron acceptor in the ground electronic state.[6] The delocalization of charge from the electron-rich moiety to the electron-poor carbon cage, which results in partially negatively charged fullerene moieties, is primarily responsible for the observed increase. Chemical changes including a range of organic moieties that donate electrons have therefore been investigated.[59] Extended π-conjugation and a robust donor–acceptor (D–A) design cause the linear polarizability (α) and second-order hyperpolarizability (β) to grow from **MP1** to **MP2C60**. Due to its symmetric electronic distribution and large HOMO–LUMO gap (ΔE), which restricts excitation, **MP1** exhibits the lowest NLO response. **MP2C60**, on the other hand, has a powerful push–pull mechanism that allows for intense intramolecular charge transfer (ICT) by using the TTF derivative as a strong donor and C_{60} as a strong acceptor. A LUMO on the C_{60} cage and a HOMO on the donor section are shown by FMO analysis. The two-state model states that **MP2C60**'s reduced bandgap improves the transition dipole and dipole change upon excitation, leading to better NLO performance.

By introducing a powerful electron-accepting unit, the fullerene attachment in **MP1C60** creates a donor–acceptor system that facilitates intramolecular charge transfer (ICT) from the donor backbone to the fullerene acceptor. The dominating β_{xxx} tensor component reflects the fullerene's ability to increase the π-conjugation length, which facilitates electron delocalization along the molecular axis. By lowering the excitation energy across the charge-transfer pathway, this prolonged conjugation and improved ICT cause β_{tot} to increase fourfold in comparison to **MP2**. The smaller π-conjugation pathway and poorer donor–acceptor strength of **MP1C60**'s molecular framework are the main causes of its lower initial hyperpolarizability when compared to **MP2C60**.

MP2C60 has a longer, electron-rich donor system that is connected to the C_{60} electron-acceptor moiety, which enables a much larger and more effective intramolecular charge transfer (ICT). The first-order hyperpolarizability is a nonlinear property that increases exponentially with the distance from which electrons can be displaced. **MP1C60**'s shorter bridge and smaller donor moiety restrict the amount of electronic polarization, despite having the same potent fullerene acceptor. As a result, **MP2C60** has a big β_{xxx} tensor component and a total β value that is more than thirteen times greater than that of **MP1C60**. This indicates both more structural asymmetry and greater electronic polarization due to enhanced intramolecular charge transfer. Overall, the remarkable improvement in the hyperpolarizability of **MP1C60** and **MP2C60** is mostly caused by the addition of fullerene to these molecules, as well as ideal donor–acceptor geometries and prolonged conjugation. Of the systems under study, **MP2C60** has the highest polarizability and hyperpolarizability, making it the most promising option for nonlinear optical applications, as shown in Table 5.

The reported NLO coefficients have been theoretically calculated using DFT/TD-DFT methods, and no experimental measurements have been performed; experimental verification is suggested as future work. However, the suggested Zn porphyrin–bridge–fullerene molecules can be produced by attaching stiff ethynyl spacers and thiophene units to the porphyrin

Table 5 HOMO–LUMO energies, bandgap, polarizability (α), and hyperpolarizability ($\beta \times 10^{-30}$ esu) of MP1, **MP2**, **MP1C60**, and **MP2C60**

Comp.	MP1	MP2	MP1C60	MP2C60
HOMO (eV)	−10.877	−9.369	−9.162	−8.220
LUMO (eV)	−9.796	−8.933	−8.244	−7.507
Bandgap (eV)	1.081	0.436	0.918	0.714
Polarizability (α) (1×10^{-30} esu)	8.74	19.91	14.05	50.73
Hyperpolarizability (β) (1×10^{-30} esu)	0.00524	1395.54	5712.68	78 128.92

core by well-known palladium-catalyzed cross-coupling processes, such as Sonogashira or Suzuki reactions. The carbon cage can then be precisely functionalized by covalently joining the fullerene (C_{60}) moiety *via* high-yield ''click-like'' reactions like the Bingel reaction or the Prato reaction. The conjugation length and donor–acceptor distance, which are critical for adjusting the nonlinear optical (NLO) characteristics and guaranteeing the stability of the finished composite, can be precisely controlled using these modular synthetic approaches.

In a related study, the first-order hyperpolarizability (β) of *para*-aminobenzoic acid is 29.99×10^{-30} esu, indicating moderate nonlinear optical (NLO) behavior.[60] In contrast, the **MP2C60** system exhibits a significantly higher β of $78\,128.92 \times 10^{-30}$ esu, an enhancement of approximately 2600-fold due to strong intramolecular charge transfer, extended π-conjugation, and a smaller band gap (0.714 eV). Urea–barbituric acid (UBA) crystals that have been investigated experimentally exhibit significant third-order NLO activity and effective optical limiting, but their high band gap ($\sim$4.50 eV) restricts charge transfer, decreasing first-order hyperpolarizability.[61] Excellent third-order NLO capabilities are also displayed by morphology-dependent MoS_2 nanoplatelets, which have a low optical limiting threshold (0.73×10^{12} W m^{-2}) and a high nonlinear absorption coefficient (5.9×10^{-10} m W^{-1}).[62] Overall, UBA and MoS_2 are very successful in third-order nonlinear absorption-based optical limiting, highlighting distinct NLO regimes, but **MP2C60** is superior in second-order NLO response.

5. Conclusion

The bandgaps, polarizabilities, and first-order hyperpolarizabilities of **MP1**, **MP2**, **MP1C60**, and **MP2C60** were used to study their NLO characteristics. Because of its stiff electron cloud and little intramolecular charge transfer, **MP1** exhibits the highest bandgap and minimum polarizability, leading to negligible hyperpolarizability. **MP2**, which has moderate polarizability and a narrower bandgap, shows a notable increase in β because of higher electron delocalization and donor–acceptor alignment. NLO responsiveness is significantly improved by fullerene connection in **MP1C60** and **MP2C60**. Extended π-conjugation and fullerene-induced charge transfer cause **MP1C60** to exhibit higher β, whereas excellent donor–acceptor geometry, extended conjugation, and greatly delocalized electrons cause **MP2C60** to exhibit the highest β. These findings demonstrate that while bandgap affects NLO behavior, the main determinants of first-order hyperpolarizability are charge-transfer efficiency, conjugation duration, and molecular structure, which makes **MP2C60** an extremely interesting option for nonlinear optical uses.

Conflicts of interest

There are no conflicts to declare.

Data availability

The data that support the findings of this study are available from the corresponding author *via* email.

Acknowledgements

The authors acknowledge the support provided by the President's International Fellowship Initiative (PIFI) Project No. 2024VEA0015 of the Chinese Academy of Sciences (CAS).

References

1 S. Suresh, A. Ramanand, D. Jayaraman and P. Mani, Review on theoretical aspect of nonlinear optics, *Rev. Adv. Mater. Sci.*, 2012, **30**(2), 175–183.
2 M. U. Khan, M. Khalid, S. Asim, Momina, R. Hussain, K. Mahmood and C. Lu, *et al.*, Exploration of nonlinear optical properties of triphenylamine-dicyanovinylene coexisting donor–π–acceptor architecture by the modification of π-conjugated linker, *Front. Mater.*, 2021, **8**, 719971.
3 D. N. Christodoulides, I. C. Khoo, G. J. Salamo, G. I. Stegeman and E. W. Van Stryland, Nonlinear refraction and absorption: mechanisms and magnitudes, *Adv. Opt. Photonics*, 2010, **2**(1), 60–200.
4 V. Kumar, Linear and Nonlinear Optical Properties of Graphene: A Review, *J. Electron. Mater.*, 2021, **50**(7), 3773–3799.
5 J. W. You, S. R. Bongu, Q. Bao and N. C. Panoiu, Nonlinear optical properties and applications of 2D materials: theoretical and experimental aspects, *Nanophotonics*, 2018, **8**(1), 63–97.
6 O. Loboda, R. Zalesny, A. Avramopoulos, J. M. Luis, B. Kirtman, N. Tagmatarchis and M. G. Papadopoulos, *et al.*, Linear and nonlinear optical properties of [60] fullerene derivatives, *J. Phys. Chem. A*, 2009, **113**(6), 1159–1170.
7 F. Limosani, R. Carcione and F. Antolini, Formation of CdSe quantum dots from single source precursor obtained by thermal and laser treatment, *J. Vac. Sci. Technol., B:Nanotechnol. Microelectron.:Mater., Process., Meas., Phenom.*, 2020, **38**, 1.

8 F. Antolini, F. Limosani and R. Carcione, Direct Laser Patterning of CdTe QDs and Their Optical Properties Control through Laser Parameters, *Nanomaterials*, 2022, **12**(9), 1551.
9 F. Limosani, F. Tessore, A. Forni, A. Lembo, G. Di Carlo, C. Albanese and P. Tagliatesta, *et al.*, Nonlinear Optical Properties of Zn (II) Porphyrin, Graphene Nanoplates, and Ferrocene Hybrid Materials, *Materials*, 2023, **16**(15), 5427.
10 A. J. Garza, O. I. Osman, N. A. Wazzan, S. B. Khan, A. M. Asiri and G. E. Scuseria, A computational study of the nonlinear optical properties of carbazole derivatives: theory refines experiment, *Theor. Chem. Acc.*, 2014, **133**(4), 1458.
11 R. L. Zhong, S. L. Sun, H. L. Xu, Y. Q. Qiu and Z. M. Su, Helical carbon segment in carbon–boron–nitride heteronanotubes: structure and nonlinear optical properties, *ChemPlusChem*, 2014, **79**(5), 732–736.
12 M. R. S. A. Janjua, Nonlinear optical response of a series of small molecules: quantum modification of π-spacer and acceptor, *J. Iran. Chem. Soc.*, 2017, **14**(9), 2041–2054.
13 M. R. S. A. Janjua, Z. H. Yamani, S. Jamil, A. Mahmood, I. Ahmad, M. Haroon and S. Pan, *et al.*, First principle study of electronic and non-linear optical (NLO) properties of triphenylamine dyes: interactive design computation of new NLO compounds, *Aust. J. Chem.*, 2016, **69**(4), 467–472.
14 M. R. S. A. Janjua, A. Mahmood, M. F. Nazar, Z. Yang and S. Pan, Electronic absorption spectra and nonlinear optical properties of ruthenium acetylide complexes: a DFT study toward the designing of new high NLO response compounds, *Acta Chim. Slov.*, 2014, **61**(2), 382–390.
15 S. A. Siddiqui, T. Rasheed, M. Faisal, A. K. Pandey and S. B. Khan, Electronic structure, nonlinear optical properties, and vibrational analysis of gemifloxacin by density functional theory, *J. Spectrosc.*, 2012, **27**(3), 185–206.
16 J. H. Chou, M. E. Kosal, H. S. Nalwa, N. A. Rakow and K. S. Suslick, Applications of porphyrins and metalloporphyrins to materials chemistry, *Porphyrin Handb.*, 2000, **6**, 43–131.
17 L. K. Yan, A. Pomogaeva, F. L. Gu and Y. Aoki, Theoretical study on nonlinear optical properties of metalloporphyrin using elongation method, *Theor. Chem. Acc.*, 2010, **125**(3), 511–520.
18 M. Pizzotti, E. Annoni, R. Ugo, S. Bruni, S. Quici, P. Fantucci and M. D. Zoppo, *et al.*, A multitechnique investigation of the second order NLO response of a 10, 20-diphenylporphyrinato nickel (II) complex carrying a phenylethynyl based push-pull system in the 5-and 15-positions, *J. Porphyrins phthalocyanines*, 2004, **8**(11), 1311–1324.
19 F. Tessore, A. Orbelli Biroli, G. Di Carlo and M. Pizzotti, Porphyrins for second order nonlinear optics (NLO): an intriguing history §, *Inorganics*, 2018, **6**(3), 81.
20 A. Nayak, J. Park, K. De Mey, X. Hu, T. V. Duncan, D. N. Beratan and M. J. Therien, *et al.*, Large hyperpolarizabilities at telecommunication-relevant wavelengths in donor–acceptor–donor nonlinear optical chromophores, *ACS Cent. Sci.*, 2016, **2**(12), 954–966.
21 D. Koszelewski, A. Nowak-Król, M. Drobizhev, C. J. Wilson, J. E. Haley, T. M. Cooper and D. T. Gryko, *et al.*, Synthesis and linear and nonlinear optical properties of low-melting π-extended porphyrins, *J. Mater. Chem. C*, 2013, **1**(10), 2044–2053.
22 N. Hou, T. T. Liu and X. H. Fang, A comparative study on nonlinear optical properties of zinc porphyrins analogs: Coordination atoms and group effects, *Int. J. Quantum Chem.*, 2023, **123**(11), e27104.
23 G. Di Carlo, M. Pizzotti, S. Righetto, A. Forni and F. Tessore, Electric-field-induced second harmonic generation nonlinear optic response of A4 β-pyrrolic-substituted ZnII porphyrins: When cubic contributions cannot be neglected, *Inorg. Chem.*, 2020, **59**(11), 7561–7570.
24 N. Islam and S. S. Chimni, Geometrical structure and nonlinear response variations of metal (M= Ni2 +, Pd2 +, Pt2 +) octaphyrin complex derivatives: A DFT study, *J. Coord. Chem.*, 2017, **70**(7), 1221–1236.
25 M. T. Aziz, W. A. Gill, M. K. Khosa, S. Jamil and M. R. S. A. Janjua, Adsorption of molecular hydrogen (H 2) on a fullerene (C 60) surface: insights from density functional theory and molecular dynamics simulation, *RSC Adv.*, 2024, **14**(49), 36546–36556.
26 J. Camacho Gonzalez, S. Mondal, F. Ocayo, R. Guajardo-Maturana and A. Muñoz-Castro, Nature of C60 and C70 fullerene encapsulation in a porphyrin-and metalloporphyrin-based cage: Insights from dispersion-corrected density functional theory calculations, *Int. J. Quantum Chem.*, 2020, **120**(3), e26080.
27 E. F. Sheka, *Fullerene nanoscience: nanochemistry, nanomedicine, nanophotonics, nanomagnetism*, 2011, CRC, Boca Raton.
28 A. Hirsch and M. Brettreich, *Fullerenes: chemistry and reactions*, 2006, John Wiley & Sons.
29 P. Schwerdtfeger, L. N. Wirz and J. Avery, The topology of fullerenes, *Wiley Interdiscip. Rev.: Comput. Mol. Sci.*, 2015, **5**(1), 96–145.
30 O. Berné and A. G. Tielens, Formation of buckminsterfullerene (C60) in interstellar space, *Proc. Natl. Acad. Sci. U. S. A.*, 2012, **109**(2), 401–406.
31 J. Cami, J. Bernard-Salas, E. Peeters and S. E. Malek, Detection of C60 and C70 in a young planetary nebula, *Science*, 2010, **329**(5996), 1180–1182.
32 R. Signorini, R. Bozio and M. Prato, Optical limiting applications, in *Fullerenes: from synthesis to optoelectronic properties*, Springer Netherlands, Dordrecht, 2002, pp. 295–326.
33 L. U. I. S. Echegoyen, F. R. A. N. Ç. O. I. S. Diederich and L. E. Echegoyen, *Electrochemistry of fullerenes*, John Wiley & Sons, Inc., New York, 2000, pp. 1–51.
34 P. P. Shanbogh and N. G. Sundaram, Fullerenes revisited: Materials chemistry and applications of C60 molecules, *Resonance*, 2015, **20**(2), 123–135.
35 S. Das, D. Alagarasan, S. Varadharajaperumal, R. Ganesan and R. Naik, Tuning the nonlinear susceptibility and linear parameters upon annealing Ag 60− x Se 40 Te x nanostructured films for nonlinear and photonic applications, *Mater. Adv.*, 2022, **3**(20), 7640–7654.
36 T. T. Ngo, G. Lozano and H. Míguez, Enhanced upconversion photoluminescence in fluoride–oxyfluoride

nanophosphor films by embedding gold nanoparticles, *Mater. Adv.*, 2022, **3**(10), 4235–4242.

37 W. Deng, Z. Zhu, Y. Sun, H. Xu, S. Liu and H. Wen, Recent advances in {P 4 Mo 6}-based polyoxometalates, *Polyoxometalates*, 2024, **3**(4), 9140071.

38 P. Sanwal, A. Raza, Y. X. Miao, B. Lumbers and G. Li, Advances in coinage metal nanoclusters: From synthesis strategies to electrocatalytic performance, *Polyoxometalates*, 2024, **3**(3), 9140057.

39 R. Y. Chen, Y. P. He and J. Zhang, Combining Ti4 (embonate) 6 cages and [Pb4 (OH) 4] 4+ clusters for enhanced third-order nonlinear optical property, *Polyoxometalates*, 2022, **1**(1), 9140002.

40 K. Zhou, L. K. Yan, Y. Geng, J. Y. Ji, X. L. Wang, Z. M. Su and Z. G. Xiao, The interesting luminescence behavior and rare nonlinear optical properties of the {Ag 55 Mo 6} nanocluster, *RSC Adv.*, 2021, **11**(61), 38814–38819.

41 T. Y. Ma, T. Zhang, B. Zhu, L. K. Yan and Z. M. Su, Theoretical studies on oxidation-switchable second-order nonlinear optical responses of Metallosalen-Keggin polyoxometalate derivatives, *RSC Adv.*, 2016, **6**(58), 53438–53443.

42 A. Rana, S. Pathak, K. Kumar, A. Kumari, S. Chopra, M. Kumar and S. N. Sharma, *et al.*, Multifaceted properties of TiO 2 nanoparticles synthesized using Mangifera indica and Azadirachta indica plant extracts: antimicrobial, antioxidant, and non-linear optical activity investigation for sustainable agricultural applications, *Mater. Adv.*, 2024, **5**(7), 2767–2784.

43 M. J. Frisch, G. W. Trucks, H. B. Schlegel, G. E. Scuseria, M. A. Robb and J. R. Cheeseman, *et al.*, *Gaussian 09, Revision D.01*, Gaussian, Inc., Wallingford (CT), 2013.

44 S. A. Halim, M. A. Ibrahim, N. Roushdy, A. A. M. Farag, Y. Gabr and S. Said, Spectroscopic and TD-DFT investigations of 4-{[(2-amino-6-methylchromon-3-yl) methylidene] amino}-6-methyl-3-thioxo-3, 4-dihydro-1, 2, 4-triazin-5 (2H)-one, and its application for photovoltaic devices, *Mater. Chem. Phys.*, 2018, **217**, 403–411.

45 A. A. M. Farag, N. Roushdy, S. A. Halim, N. M. El-Gohary, M. A. Ibrahim and S. Said, Synthesis, molecular, electronic structure, linear and non-linear optical and phototransient properties of 8-methyl-1, 2-dihydro-4H-chromeno [2, 3-b] quinoline-4, 6 (3H)-dione (MDCQD): Experimental and DFT investigations, *Spectrochim. Acta, Part A*, 2018, **191**, 478–490.

46 J. S. Al-Otaibi, Y. S. Mary, Y. S. Mary, M. Krátký, J. Vinsova and M. C. Gamberini, DFT, TD-DFT and SERS analysis of a bioactive benzohydrazide's adsorption in silver hydrosols at various concentrations, *J. Mol. Liq.*, 2023, **373**, 121243.

47 A. A. El-Saady, N. Roushdy, A. A. M. Farag, M. M. El-Nahass and D. M. Abdel Basset, Exploring the molecular spectroscopic and electronic characterization of nanocrystalline Metal-free phthalocyanine: a DFT investigation, *Opt. Quantum Electron.*, 2023, **55**(7), 662.

48 M. Haroon and M. R. S. A. Janjua, Computationally assisted design and prediction of remarkably boosted NLO response of organoimido-substituted hexamolybdates, *J. Phys. Org. Chem.*, 2022, **35**, e4353.

49 S. Liu, F. W. Gao, H. L. Xu and Z. M. Su, Transition metals doped fullerenes: structures–NLO property relationships, *Mol. Phys.*, 2019, **117**(6), 705–711.

50 F. W. Gao, R. L. Zhong, S. L. Sun, H. L. Xu, L. Zhao and Z. M. Su, Charge transfer and first hyperpolarizability: cage-like radicals C59X and lithium encapsulated Li@ C59X (X= B, N), *J. Mol. Model.*, 2015, **21**(10), 258.

51 L. J. Wang, R. L. Zhong, S. L. Sun, H. L. Xu, X. M. Pan and Z. M. Su, The V-shaped polar molecules encapsulated into C s (10528)-C 72: stability and nonlinear optical response, *Dalton Trans.*, 2014, **43**(25), 9655–9660.

52 A. Karakas, A. Elmali and H. Unver, Linear optical transmission measurements and computational study of linear polarizabilities, first hyperpolarizabilities of a dinuclear iron (III) complex, *Spectrochim. Acta, Part A*, 2007, **68**(3), 567–572.

53 S. A. Halim and M. A. Ibrahim, Synthesis, spectral analysis, quantum studies, NLO, and thermodynamic properties of the novel 5-(6-hydroxy-4-methoxy-1-benzofuran-5-ylcarbonyl)-6-amino-3-methyl-1 H-pyrazolo [3, 4-b] pyridine (HMBPP), *RSC Adv.*, 2022, **12**(21), 13135–13153.

54 C. Liang, X. Cui, W. Dong, J. Qin and Q. Duan, Enhanced non-linear optical properties of porphyrin-based polymers covalently functionalized with graphite phase carbon nitride, *Front. Chem.*, 2022, **10**, 1102666.

55 D. Kamli, D. Hannachi, D. Samsar and H. Chermette, Bis-TTF-Ge derivatives: promising linear and nonlinear optical properties, a theoretical investigation, *New J. Chem.*, 2023, **47**(3), 1234–1246.

56 D. Zhao, X. He, P. W. Ayers and S. Liu, Excited-state polarizabilities: a combined density functional theory and information-theoretic approach study, *Molecules*, 2023, **28**(6), 2576.

57 A. Ahsin, I. Ejaz, S. Sarfaraz, K. Ayub and H. Ma, Polaron formation in conducting polymers: a novel approach to designing materials with a larger NLO response, *ACS Omega*, 2024, **9**(12), 14043–14053.

58 P. Macchi, Polarizabilities of Atoms in Molecules: Choice of the Partitioning Scheme and Applications for Secondary Interactions, *Molecules*, 2025, **30**(20), 4137.

59 F. Limosani, F. Tessore, G. Di Carlo, A. Forni and P. Tagliatesta, Nonlinear optical properties of porphyrin, fullerene and ferrocene hybrid materials, *Materials*, 2021, **14**(16), 4404.

60 S. Lakhera, M. Rana, K. Devlal, S. Sharma, P. Chowdhury, V. Dhuliya and T. S. Girisun, *et al.*, Exploring the nonlinear optical limiting activity of para-aminobenzoic acid by experimental and DFT approach, *J. Photochem. Photobiol., A*, 2023, **444**, 114987.

61 A. Suresh, R. M. Jauhar, T. S. Girisun, N. Manikandan and G. Vinitha, Third order nonlinearity examined by pulsed and CW lasers: an organic urea barbituric acid (UBA) single crystal for optical limiting application with DFT study, *Mater. Res. Express*, 2024, **11**(1), 016203.

62 M. Durairaj, T. C. Sabari Girisun and A. G. Al-Sehemi, Impact of morphology on the nonlinear optical absorption of pristine molybdenum disulfide (MoS_2) nanostructures, *Opt. Mater.*, 2022, **131**, 112632.